

ARTICLE

Open Access

# Tuning of oscillation modes by controlling dimensionality of spin structures

Hee-Sung Han<sup>1,2</sup>, Sooseok Lee<sup>2</sup>, Min-Seung Jung<sup>3</sup>, Namkyu Kim<sup>2</sup>, Dae-Han Jung<sup>2</sup>, Myeonghwan Kang<sup>2</sup>, Hye-Jin Ok<sup>2</sup>, Weilun Chao<sup>1</sup>, Young-Sang Yu<sup>4,5</sup>, Jung-Il Hong<sup>3</sup>, Mi-Young Im<sup>1</sup> and Ki-Suk Lee<sup>2</sup>

## Abstract

Harmonic oscillation of spin structures is a physical phenomenon that offers great potential for applications in nanotechnologies such as nano-oscillators and bio-inspired computing. The effective tuning of oscillations over wide frequency ranges within a single ferromagnetic nanoelement is a prerequisite to realize oscillation-based nanodevices, but it has not been addressed experimentally or theoretically. Here, utilizing a vortex core structure, one of spin structures, we report a drastic change of oscillation modes over the frequency range from MHz to sub-GHz in a 100 nm-thick permalloy circular disk. Oscillation mode was found to considerably depend on the shape and dimension of the vortex core structure and various oscillation modes over a wide range of frequencies appeared with dimensional change in the vortex core structure. This work demonstrates that oscillation modes of the vortex core structure can be effectively tuned and opens a way to apply spin structures to oscillation-based technology.

## Introduction

Harmonic oscillation is an intriguing physical phenomenon that has attracted significant attentions in various material systems. The fundamental understanding and manipulation of oscillation properties (e.g., frequency and amplitude) have been extensively studied in the research fields of two-dimensional (2D) materials<sup>1–3</sup>, quantum materials<sup>4,5</sup>, lattice distortion<sup>6,7</sup> and magnetic materials<sup>8–10</sup> since it offers a high potential for energy-efficient technological applications, e.g., nano-oscillators<sup>1,2,11–13</sup>, bio-inspired computing<sup>5,14–18</sup>, and programmable logic devices<sup>19,20</sup>.

Spin structures have been highly regarded in the application to oscillation-based nanodevices due to its high stability and rich oscillation properties<sup>21–28</sup>. The magnetic vortex, one of spin structures, is a ground state stabilized in a soft ferromagnetic disk, which is composed

of the in-plane curling magnetization and out-of-plane magnetization at the centre of the element, referred to as a vortex core. The vortex core structure in typical thin ferromagnetic disks where the thickness is within the range of the exchange length (thickness < 50 nm) is considered as a rigid structure and it generally shows the gyrotropic motion of the MHz-ranged frequency without its deformation along the thickness direction, which is called the zeroth-order gyrotropic mode<sup>29–32</sup>. The oscillation mode of vortex core structure can be easily detected through the electrical measurements compared to the oscillation mode of other spin structures due to its large amplitude and narrow linewidth<sup>11–13</sup>. Recently, it has been revealed that the oscillation mode could significantly change as the thickness of the disk increases and it leads to the emergence of unique three-dimensional (3D) dynamic characteristics of magnetic vortex<sup>33–41</sup>. For instance, the higher-order gyrotropic modes with GHz frequency range accompanying oscillation nodes along the thickness of the disk appear in addition to zeroth-order gyrotropic modes<sup>38–41</sup>.

To realize a versatile nano-oscillator, efficient tuning of harmonic oscillations of vortex core structure in a wide

Correspondence: Mi-Young Im (mim@lbl.gov) or Ki-Suk Lee (kisuk@unist.ac.kr)

<sup>1</sup>Center for X-ray Optics, Lawrence Berkeley National Laboratory, Berkeley, CA 94720, USA

<sup>2</sup>Department of Materials Science and Engineering, Ulsan National Institute of Science and Technology (UNIST), Ulsan 44919, Republic of Korea  
Full list of author information is available at the end of the article

© The Author(s) 2022



**Open Access** This article is licensed under a Creative Commons Attribution 4.0 International License, which permits use, sharing, adaptation, distribution and reproduction in any medium or format, as long as you give appropriate credit to the original author(s) and the source, provide a link to the Creative Commons license, and indicate if changes were made. The images or other third party material in this article are included in the article's Creative Commons license, unless indicated otherwise in a credit line to the material. If material is not included in the article's Creative Commons license and your intended use is not permitted by statutory regulation or exceeds the permitted use, you will need to obtain permission directly from the copyright holder. To view a copy of this license, visit <http://creativecommons.org/licenses/by/4.0/>.

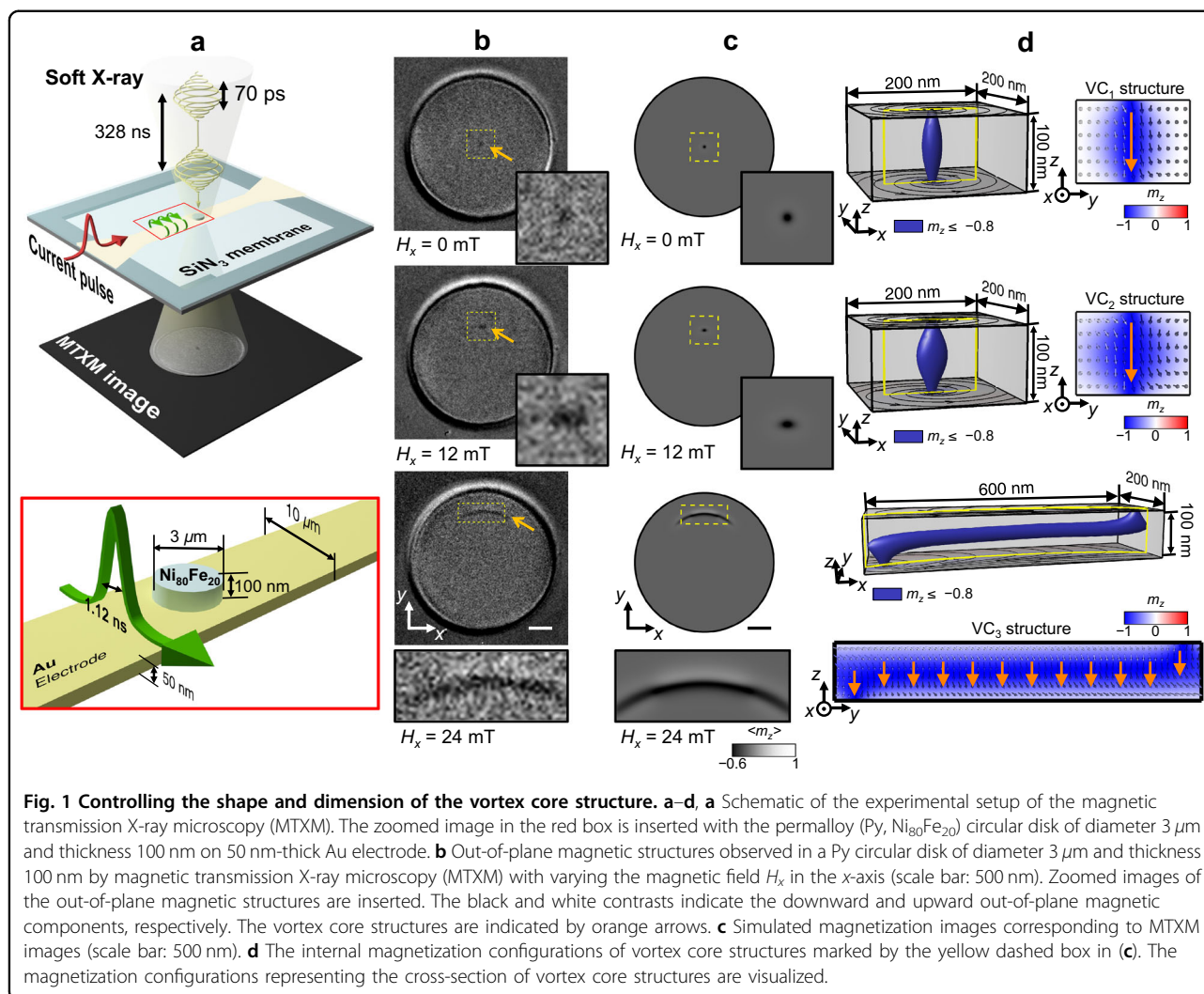


**Fig. 1 Controlling the shape and dimension of the vortex core structure.** **a–d**, **a** Schematic of the experimental setup of the magnetic transmission X-ray microscopy (MTXM). The zoomed image in the red box is inserted with the permalloy (Py,  $\text{Ni}_{80}\text{Fe}_{20}$ ) circular disk of diameter  $3\ \mu\text{m}$  and thickness  $100\ \text{nm}$  on  $50\ \text{nm}$ -thick Au electrode. **b** Out-of-plane magnetic structures observed in a Py circular disk of diameter  $3\ \mu\text{m}$  and thickness  $100\ \text{nm}$  by magnetic transmission X-ray microscopy (MTXM) with varying the magnetic field  $H_x$  in the  $x$ -axis (scale bar:  $500\ \text{nm}$ ). Zoomed images of the out-of-plane magnetic structures are inserted. The black and white contrasts indicate the downward and upward out-of-plane magnetic components, respectively. The vortex core structures are indicated by orange arrows. **c** Simulated magnetization images corresponding to MTXM images (scale bar:  $500\ \text{nm}$ ). **d** The internal magnetization configurations of vortex core structures marked by the yellow dashed box in (c). The magnetization configurations representing the cross-section of vortex core structures are visualized.

range of frequencies, especially in a single ferromagnetic element is highly required<sup>31,42,43</sup>. However, earlier works on the oscillation of vortex core structure have focused on tuning the eigenfrequency of the zeroth-order gyrotropic mode of vortex core structure in thin ferromagnetic disks, and thus the reported frequency tuning range has been limited to MHz range<sup>31,42,43</sup>. In our works, we manipulate oscillation modes of vortex core structure over from MHz to sub-GHz frequency range within a  $100\ \text{nm}$ -thick single permalloy ( $\text{Ni}_{80}\text{Fe}_{20}$ , Py) circular disk utilizing time-resolved magnetic transmission X-ray microscopy (MTXM) measurement (See Fig. 1a). We show that the oscillation modes of the vortex core structure are controllable by manipulating the shape and dimension of the vortex core structure.

## Results

### Manipulating the shape and dimension of the vortex core structure

Figure 1b shows three different magnetic structures imaged at the external magnetic fields of  $H_x = 0\ \text{mT}$ ,

$12\ \text{mT}$ , and  $24\ \text{mT}$  in permalloy ( $\text{Ni}_{80}\text{Fe}_{20}$ , Py) circular disk of diameter  $D = 3\ \mu\text{m}$  and thickness  $h = 100\ \text{nm}$  by utilizing MTXM (See Methods)<sup>44</sup>. Black and white contrasts in those images indicate downward and upward magnetic components, respectively. At zero field ( $H_x = 0\ \text{mT}$ ), a black spot at the centre of the disk is observed, which corresponds to the typical dot-shaped vortex core structure with downward magnetization. As  $H_x$  increase to  $+12\ \text{mT}$ , the vortex core structure is shifted in the  $+y$ -axis and the vortex core structure gets slightly enlarged in a horizontal direction. As  $H_x$  increases further, the vortex core structure gets closer to the edge of the disk and completely deforms into the elongated structure with curvature (See the magnetic image at  $H_x = +24\ \text{mT}$  in Fig. 1b). The magnetic images in Fig. 1b show that the shape and dimension of the vortex core structure noticeably change as it gets closer to the edge of the disk by increasing the external magnetic field (See zoomed images). Figure 1c indicates the simulated magnetic structures (See Methods)<sup>45</sup>, which match well with the experimentally observed structures.

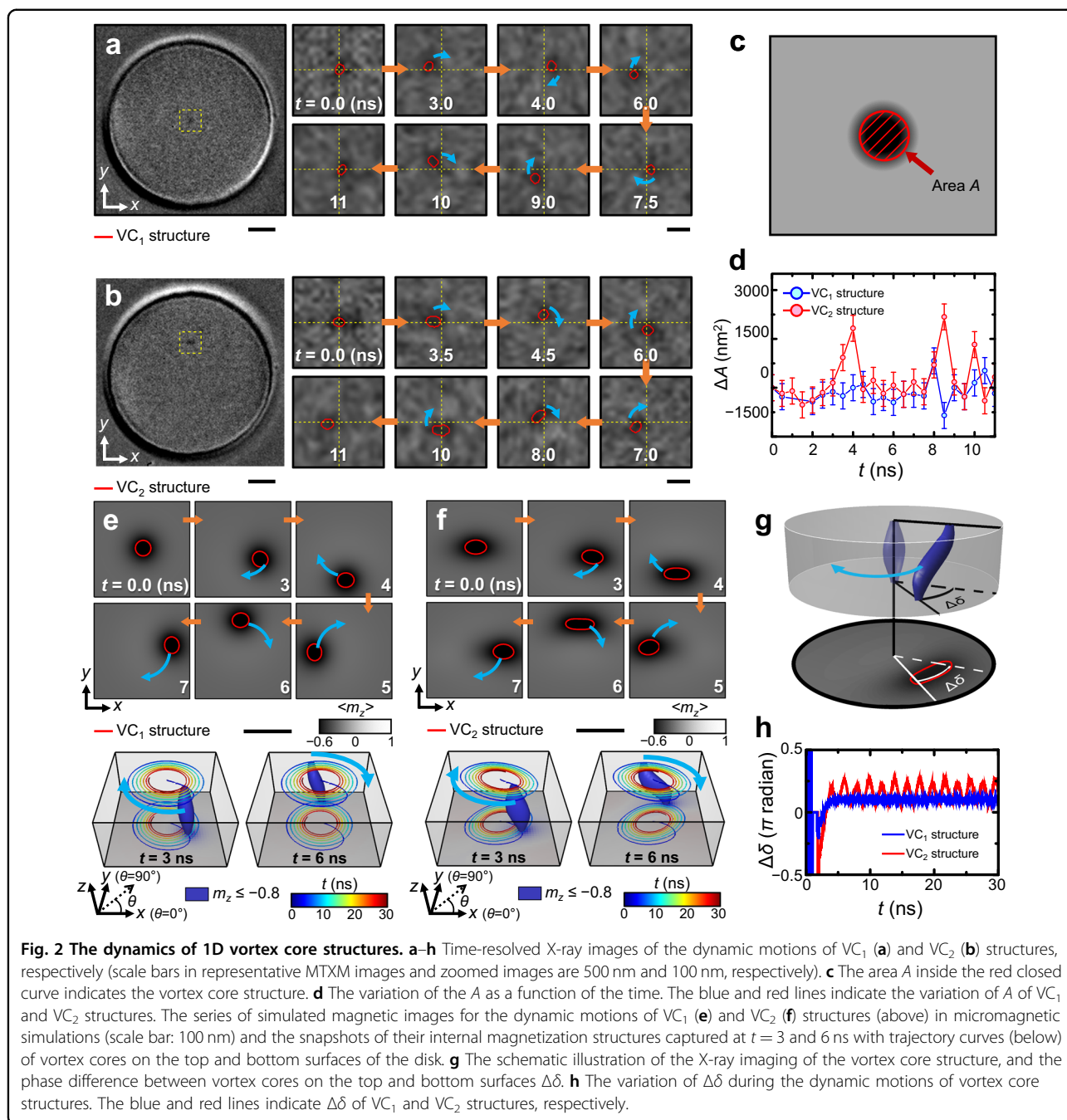
The detailed 3D magnetization configurations of vortex core structures (marked by the yellow dashed box in Fig. 1c) are displayed in Fig. 1d. The volumes of vortex core structures with  $m_z \leq -0.8$  are indicated by blue color. One can see that as the field varies, the shape of the vortex core structure changes and the vortex core structure is transformed from a one-dimensional (1D) vortex core structure to a 2D vortex core structure containing a domain wall. At  $H_x = 0$  mT, a typical 1D vortex core structure (hereafter, called VC<sub>1</sub> structure) is observed; the vortex cores on the top and bottom surfaces are coaxially aligned, which supports that the VC<sub>1</sub> structure is a 1D vortex core structure (See orange dotted arrow). In the vortex core structure at  $H_x = 12$  mT (hereafter, called VC<sub>2</sub> structure), the vortex cores on top and bottom surfaces are still coaxially aligned like VC<sub>1</sub> structure, which supports that VC<sub>2</sub> structure is also a 1D structure (See orange dotted arrow). However, unlike VC<sub>1</sub> structure, the shape of VC<sub>2</sub> structure is slightly expanded along the horizontal direction and the magnetization of the VC<sub>2</sub> structure is not completely uniform along the thickness of the disk, which might occur to compensate for the demagnetization energy induced by the vortex core structure shifting toward the edge of the disk. At  $H_x = 24$  mT, the vortex core structure (hereafter, called VC<sub>3</sub> structure) is largely deformed. The vortex cores located on the top and bottom surfaces of the disk are no longer coaxial and the two vortex cores on the top and bottom surfaces of the disk are connected through the domain wall stretched along the  $x$ -axis (See Supplementary Fig. 1 and Supplementary Note 1), which indicates that the VC<sub>3</sub> structure is clearly a 2D vortex core structure (See orange dotted arrows)<sup>21,40,46–51</sup>. We confirmed that the dimensional change of the vortex core structure starts occurring at  $H_x = 15$  mT, and the domain wall connecting the vortex cores on the top and bottom surfaces of the disk gets longer as  $H_x$  increases until the vortex core structure is annihilated at  $H_x = 62$  mT (See Supplementary Fig. 2 and Supplementary Note 2). In addition, it was confirmed that the dimensional change of vortex core structure by applying magnetic field only occurs when the disk is thicker than or equal to 70 nm in the Py circular disk of  $D = 3 \mu\text{m}$  (See Supplementary Fig. 2 and Supplementary Note 2). It is noticed that the observed dimensional change of vortex core structure is analogous to the one achieved by changing the geometry of the disk from square to the rectangle<sup>51</sup>. The results in Fig. 1 demonstrate that the shape and dimension of vortex core structure in thick ferromagnetic disks can be controlled simply by applying in-plane magnetic fields.

### Dynamics of 1D vortex core structures

To investigate the oscillation mode of vortex core structures formed with varying external magnetic fields,

we performed time-resolved MTXM measurements<sup>44</sup> (See Methods). To excite the dynamic motions of the vortex core structures, we injected the magnetic field pulse with an amplitude of 1 mT and a pulse width of 1.12 ns to the disk along the  $-x$ -axis. Figure 2a, b show the representative snapshots of the dynamic motions of VC<sub>1</sub> and VC<sub>2</sub> structures, respectively. To track the position of vortex core structures, we defined area  $A$  of the vortex core structure with the normalized MTXM contrast  $< 0.2$  as denoted by the red closed curves (See Fig. 2c and Methods). Both vortex core structures show the clockwise (CW) gyrotropic motion (See Fig. 2a, b, Supplementary Movies 1, 2, and Supplementary Fig. 3). However, the shapes of the two vortex core structures become distinct from each other during their dynamic motions. The shape of the VC<sub>2</sub> structure, indicated by the red closed curves in Fig. 2b, is varied from (to) circular to (from) elliptical shape during its dynamic motion, whereas the shape of the VC<sub>1</sub> structure stays the same, circular shape over the dynamic process. To quantitatively analyze the change of shape and size of those vortex core structures, we measured the variation of  $A$  ( $\Delta A$ ) during their dynamic motions. Figure 2d clearly shows that unlike the case of the VC<sub>1</sub> structure showing subtle random fluctuations,  $\Delta A$  of the VC<sub>2</sub> structure is largely and periodically varied during its dynamic motion. It should be noticed that the noticeable changes of shape and size have never been reported in the dynamic motion of vortex core structures in typical thin ferromagnetic disks<sup>22,23</sup>.

For deeper understanding of the shape and size variation of the VC<sub>2</sub> structure, we performed micromagnetic simulations for the dynamic motions of both VC<sub>1</sub> and VC<sub>2</sub> structures (See Methods). Figure 2e, f illustrate the simulated magnetization images during the dynamic motions of VC<sub>1</sub> and VC<sub>2</sub> structures, respectively. The shape and size of the VC<sub>2</sub> structure noticeably change during the dynamic motion as observed in experiments unlike those of the VC<sub>1</sub> structure (See Fig. 2e, f, Supplementary Movies 3, 4). Detailed 3D magnetization configurations of VC<sub>1</sub> and VC<sub>2</sub> structures during their dynamic motions were investigated to clearly interpret the change of shape and size of the VC<sub>2</sub> structure seen in 2D images, respectively (See Fig. 2e, f). The respective trajectory curves of vortex core motions on the top and bottom surfaces of the disk are added. For the VC<sub>1</sub> structure, the gyrotropic motions with circular trajectories are observed in both vortex cores on the top and bottom surfaces. In the VC<sub>2</sub> structure, however, vortex cores show the gyrotropic motions with elliptical trajectories. Interestingly, the major axis of the elliptical trajectories observed in the VC<sub>2</sub> structure is aligned to the axis rotated by an angle of  $|\theta| \sim 35^\circ$  with respect to the magnetic field pulse direction ( $x$ -axis,  $|\theta| = 0^\circ$ ), which is in sharp contrast to previous reports that the major axis of



the elliptical trajectory of vortex core gyrotropic motion in off-resonance is aligned to be parallel ( $x$ -axis,  $|\theta| = 0^\circ$ ) or perpendicular ( $y$ -axis,  $|\theta| = 90^\circ$ ) to the magnetic field pulse direction ( $x$ -axis,  $|\theta| = 0^\circ$ )<sup>31,32</sup>. More importantly, the directions of major axes of the elliptical trajectories of vortex core motions on the top and bottom surfaces are not aligned. The major axis of the elliptical trajectories of the vortex cores of the top and bottom surfaces are aligned to the axis rotated by  $\theta = -35^\circ$  and  $\theta = +35^\circ$ , respectively.

It is worth noting that the vortex core on the top surface is slightly lagging behind that on the bottom surface in both VC<sub>1</sub> and VC<sub>2</sub> structure, which indicates that there is a phase difference in the gyrotropic motions of the vortex cores of the top and bottom surfaces (See Fig. 2g). The non-zero phase difference of the gyrotropic motions of vortex cores on the top and bottom surfaces causes structural strain of the vortex core structure and is reflected as a slightly inclined structure in the thickness direction<sup>34</sup>. We estimated the phase differences of the

gyrotropic motions of vortex cores on the top and bottom surfaces  $\Delta\delta$  during the dynamic motion of  $VC_1$  and  $VC_2$  structures (See Fig. 2h). In the  $VC_1$  structure, the  $\Delta\delta$  occurred between the two vortex cores on the top and bottom surfaces remains the same over the dynamic motion (See blue line in Fig. 2h). Surprisingly,  $\Delta\delta$  in  $VC_2$  structure is periodically varied during the dynamic motion of the  $VC_2$  structure (red line in Fig. 2h), which is probably due to the different directions of major axes of the elliptical trajectories of the vortex cores on the top and bottom surfaces (See Supplementary Movie 5). Based on the simulations results (See Fig. 2e–h), it can be understood that the shape and size of  $VC_1$  structure rarely varied (See Fig. 2a, d) due to the  $\Delta\delta$  remaining constant in the structure (See Fig. 2h). On the other hand, the variation of the  $\Delta\delta$  of the  $VC_2$  structure (See Fig. 2h) causes the periodic shape change of the  $VC_2$  structure from (to) circular to (from) elliptical shape as shown in Fig. 2b, d.

#### Dynamics of the 2D vortex core structure

Figure 3 shows the dynamic motion of the  $VC_3$  structure, which is significantly different from those of  $VC_1$  and  $VC_2$  structures (See Fig. 3a and Supplementary Movie 6). The flexure oscillation of the  $VC_3$  structure with the lateral motion and severe shape deformation is witnessed as shown in Fig. 3a. The position and shape changes of the  $VC_3$  structure during its dynamic motion are clearly observed as seen in green areas (See right panel of Fig. 3a). In Fig. 3, the black and red curves represent the initial position of the  $VC_3$  structure at  $t = 0$  ns and its perturbed position triggered by the same magnetic field pulse applied to  $VC_1$  and  $VC_2$  structures.

Figure 3b displays the simulated magnetization image of the  $VC_3$  structure and 3D magnetization configurations during the dynamic motion. It is noticed that the domain wall portion of the  $VC_3$  structure shows the flexure oscillation as well as the lateral motion clearly visualized in experimental results (See Fig. 3a). It expands and shrinks repetitively in the horizontal direction (See Supplementary Movie 7). We traced the change of green areas in Fig. 3a, b to quantitatively estimate the position change of the  $VC_3$  structure (See Fig. 3c) and found that the position of the  $VC_3$  structure was largely fluctuated (See Fig. 3c) after the initial lateral motions triggered by magnetic field pulse injected.

Our micromagnetic simulation verified that while the domain wall portion of the  $VC_3$  structure experiences the flexure oscillation with the rigorous lateral motion (See Fig. 3b), the vortex cores on the top and bottom surfaces of the disk still show gyrotropic motions similar to those of  $VC_1$  and  $VC_2$  structures (See Fig. 3d). Figure 3d exhibits that the trajectory of the vortex core motions on the top and bottom surfaces ( $VC^{\text{Top}}$  and  $VC^{\text{Bot}}$ ) are elliptical as observed in the dynamic motion of the  $VC_2$  structure.

However, vortex cores on the top and bottom surfaces of the  $VC_3$  structure show not only the phase difference but also considerably different gyrotropic radius. Those differences of phase and gyrotropic radius of vortex cores on the top and bottom surfaces that occurred during the dynamic motion of the  $VC_3$  structure might be responsible for the flexure oscillation and shape deformation of the domain wall connecting the two cores on surfaces. As the dimension of the vortex core structure changes from 1D to 2D, the dynamic motion of the vortex core structure becomes more complex with the oscillation of the domain wall in addition to the gyrotropic motions of vortex cores on surfaces.

#### Oscillation modes of vortex core structures with different dimensions

To investigate oscillation modes of 1D and 2D vortex core structures, we obtained the fast Fourier transformation (FFT) power spectra for the  $VC_2$  and  $VC_3$  structures from experimental data taken by MTXM measurements (See Fig. 4a and Methods). The blue and red lines in Fig. 4a indicate the FFT power spectrum for the  $VC_2$  and  $VC_3$  structures, respectively. The peaks in FFT power spectra denoted by black arrows indicate individual oscillation modes of vortex core structures. It clearly shows that the number and the frequency of oscillation modes of 1D vortex core structure are different from that of 2D vortex core structure. As the dimension of the vortex core structure changes from 1D to 2D, the oscillation mode of sub-GHz frequency appears. To understand the experimentally observed tuned oscillation modes according to the dimensional change of the vortex core structures in detail, we performed micromagnetic simulations (See Fig. 4b and Methods). Figure 4b shows FFT power spectra for the vortex core structures with varying  $H_x$  obtained from the micromagnetic simulation. Each branch in FFT power spectra indicates an individual oscillation mode of vortex core structures. The frequencies of two oscillation modes in the low field region ( $H_x < 12$  mT) where  $VC_1$  structure is stabilized, are rarely changed. However, at  $12 \text{ mT} \leq H_x < 15 \text{ mT}$  where  $VC_2$  structure is formed, the frequencies of both oscillation modes alter, which suggests that the shape change of the vortex core structure such as the expansion of the core observed in  $VC_2$  structure results in the change of oscillation frequency. More importantly, the drastic change of the FFT power spectra is witnessed around  $H_x = 15$  mT where the dimensional change of the vortex core structure occurs. For 1D vortex core structures,  $VC_1$  and  $VC_2$  structures ( $H_x < 15$  mT), there are only two distinct modes denoted by  $F_0^{1D}$  and  $F_1^{1D}$  with large and small powers. When the 1D vortex core structure is transformed into the 2D vortex core structure ( $H_x > 15$  mT) and the  $VC_3$  structure is established, various oscillation modes over a

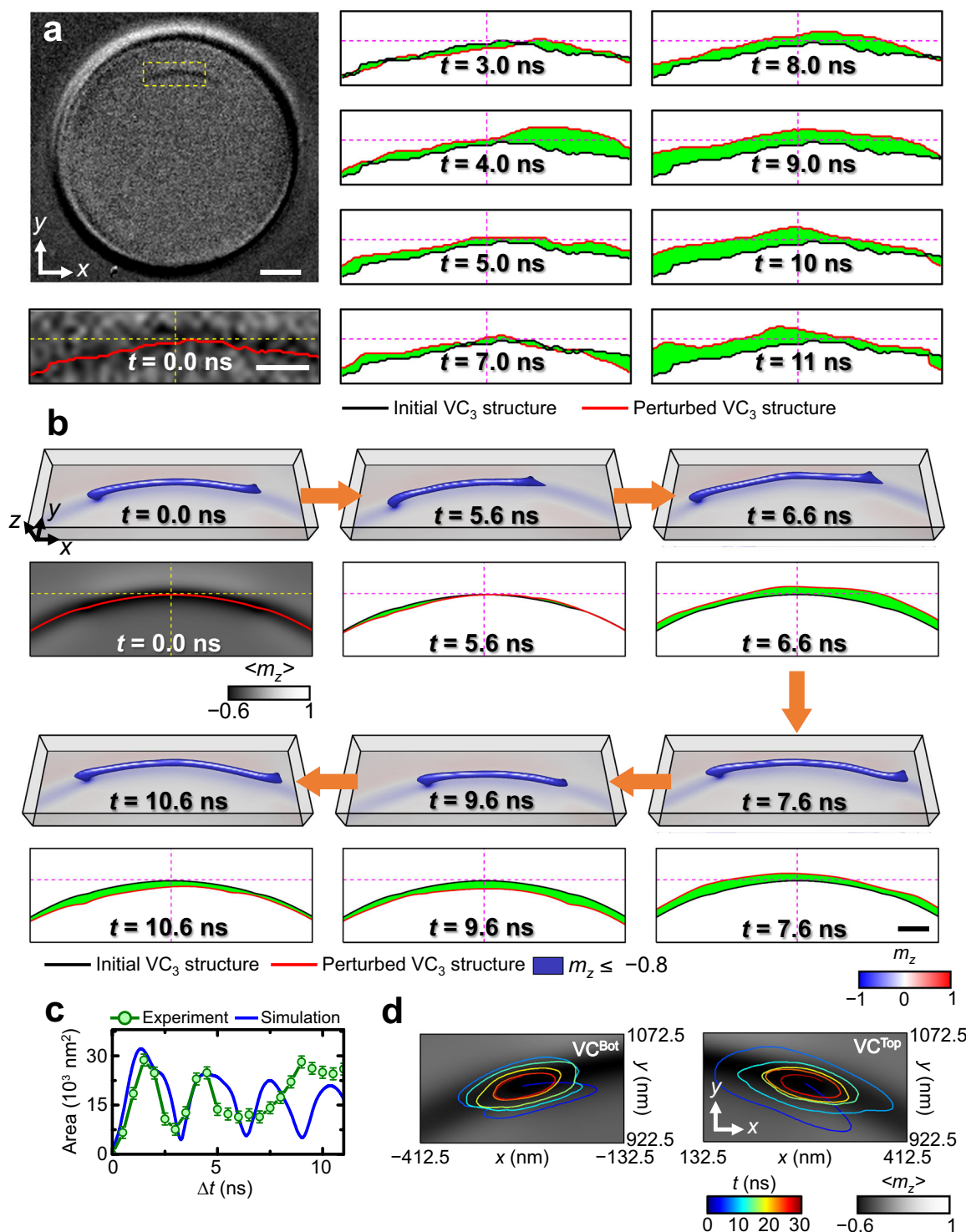


**Fig. 3** The dynamics of the 2D vortex core structure. **a–d**, **a** The series of magnetic images for the dynamic motion of the VC<sub>3</sub> structure taken by time-resolved MTXM. The black line indicates the initial position of the VC<sub>3</sub> structure at  $t = 0$  ns. (scale bars in the representative MTXM images and zoomed images: 500 nm and 300 nm, respectively). **b** The snapshot images of the 3D magnetization configurations (above) of VC<sub>3</sub> structures and the core structures (below), which were obtained from micromagnetic simulation during the dynamic motion (scale bar: 100 nm). The red lines in **(a)** and **(b)** indicate the perturbed position of the VC<sub>3</sub> structure. The area between those two lines is filled in green color. **c** The variations of the green-colored area obtained from the experiment (green line) and simulation (blue line) data in **(a)** and **(b)** which show the perturbation of the dynamic motions of the VC<sub>3</sub> structure, quantitatively. **d** The trajectory curves of vortex cores on the top and bottom surfaces of the disk obtained from the micromagnetic simulation.

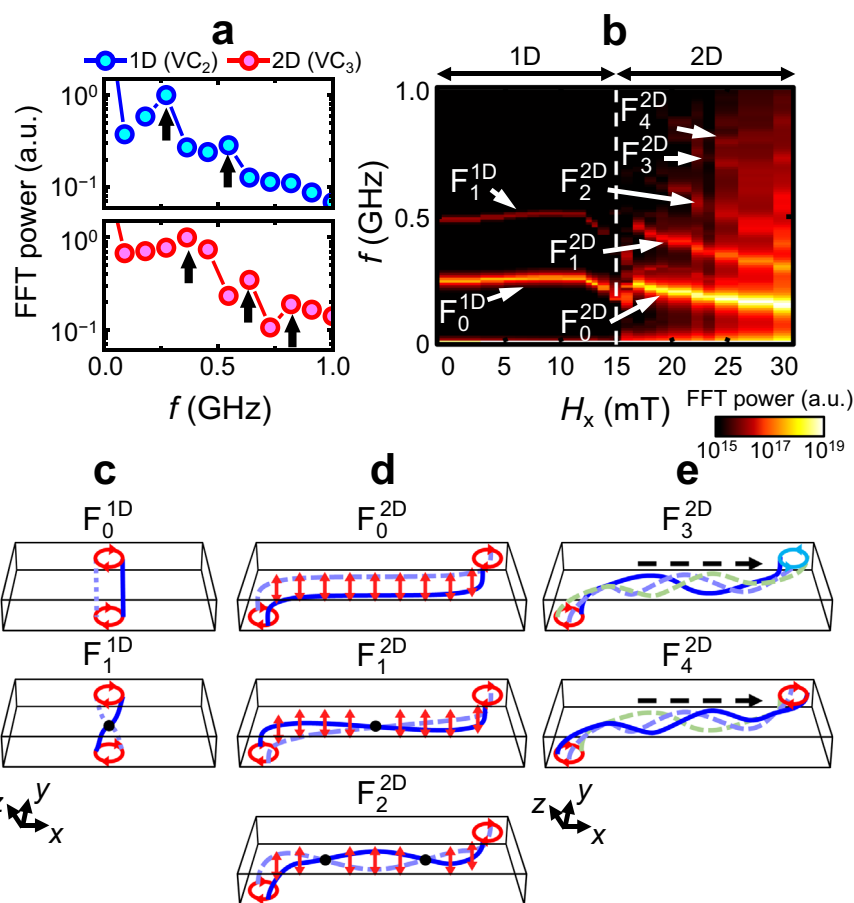


**Fig. 4** The oscillation modes of vortex core structures formed with varying the in-plane magnetic field. **a–e**, **a** The fast Fourier transformation (FFT) power spectra for the 1D and 2D vortex core structures obtained from MTXM measurements. The red and blue lines indicate the normalized FFT power spectra of VC<sub>2</sub> and VC<sub>3</sub> structures, respectively. **b** FFT power spectra for vortex core structures as function of  $H_x$  taken from micromagnetic simulation. The white dashed line indicates  $H_x = 15$  mT where the dimensional change of the vortex core structure from 1D to 2D occurs. The schematic illustrations of the zeroth- and higher-order modes of 1D ( $F_0^{1D}$ , and  $F_1^{1D}$ ) (**c**) and 2D ( $F_0^{2D}$ ,  $F_1^{2D}$ , and  $F_2^{2D}$ ) (**d**) vortex core structures. **e** The modes  $F_3^{2D}$ , and  $F_4^{2D}$  where spin-wave propagates along the domain wall of the 2D vortex core structure are schematically illustrated. The black dashed line indicates the spin-wave propagation direction. The clockwise and counter-clockwise gyrotropic motions of vortex cores on the top and bottom surfaces are denoted by the red and light blue arrows, respectively. The black dashed line indicates the spin-wave propagation direction.

wide range of frequencies from MHz to sub-GHz appear. The  $F_0^{1D}$  and  $F_1^{1D}$  modes are split into five modes, denoted by  $F_0^{2D}$ ,  $F_1^{2D}$ ,  $F_2^{2D}$ ,  $F_3^{2D}$ , and  $F_4^{2D}$  (Fig. 4b). It can be noticed that the FFT power spectrum of VC<sub>3</sub> structure obtained by micromagnetic simulations exhibits five oscillation modes, unlike experimental result that shows three oscillation modes. This is because of the better frequency resolution (0.01 GHz) of the FFT power spectra of the micromagnetic simulation than that (0.091 GHz) of the experiment (See Methods).

The modes of 1D and 2D vortex core structures are schematically illustrated in Fig. 4c–e, which were confirmed by calculating inverse FFT corresponding to each oscillation mode (See Supplementary Figs. 4, 5, Supplementary Notes 3, 4). For the 1D vortex core structure (See Fig. 4c, Supplementary Fig. 4 and Supplementary

Note 3), mode  $F_0^{1D}$  corresponds to the gyrotropic motion of the vortex core structure, which is uniformly excited in the thickness direction without any node. Mode  $F_1^{1D}$  still corresponds to the gyrotropic motion of the vortex core structure, but in this case, at the centre of the vortex core structure in the thickness direction, the gyrotropic motion is not excited due to the node formed at the centre of the vortex core structure. That is, modes  $F_0^{1D}$  and  $F_1^{1D}$  are the zeroth- and first-order gyrotropic modes of vortex core structures, respectively. The modes  $F_0^{2D}$ ,  $F_1^{2D}$ , and  $F_2^{2D}$  of 2D vortex core structures (See Fig. 4d, Supplementary Fig. 5, and Supplementary Note 4) correspond to the gyrotropic motions of vortex cores on the top and bottom surfaces as well as the lateral motion of the domain wall. Similar to the modes of the 1D vortex core structure, mode  $F_0^{2D}$  corresponds

to dynamic motion without a node, and mode  $F_1^{2D}$  represents dynamic motion including a node at the centre of the domain wall. In addition, it is found that the mode  $F_2^{2D}$  includes two nodes. Namely, the modes  $F_0^{2D}$ ,  $F_1^{2D}$ , and  $F_2^{2D}$  are the zeroth-, first-, and second-order oscillation modes of the 2D vortex core structure, respectively. The modes  $F_3^{2D}$ , and  $F_4^{2D}$  correspond to the modes where the spin-wave propagates along the domain wall while the gyrotropic motions of vortex cores occur on the top and bottom surfaces. The spin-waves in modes  $F_3^{2D}$  and  $F_4^{2D}$  have different oscillation phases from each other. In mode  $F_3^{2D}$ , the vortex cores on the top surface shows the counter-clockwise (CCW) gyrotropic motion while the vortex cores on the bottom surface shows CW gyrotropic motion. In contrast, in mode  $F_4^{2D}$ , both vortex cores on the top and bottom surfaces show CW gyrotropic motion (See Fig. 4e and Supplementary Note 4). The superposition of multiple oscillation modes is reflected by the flexure oscillation of the VC<sub>3</sub> structure including noticeable motion change observed in the experiment. The results in Fig. 4 support that the oscillation properties of vortex core structures such as eigenfrequency, the number of oscillation modes, and the range of oscillation frequency, which are important features for developing vortex-based nano-oscillator, can be easily tuned by manipulating the shape and dimension of vortex core structure within a single magnetic disk.

In summary, we demonstrate that the oscillation modes of vortex core structures can be controlled over the wide range of frequencies from MHz to sub-GHz by manipulating the shape and dimension of the vortex core structure within a single ferromagnetic disk. The observed various oscillation modes of the vortex core structure can be electrically excited by spin-transfer torque<sup>13,52</sup>. Moreover, among various oscillation modes, a specific oscillation with a desirable frequency can be amplified<sup>53,54</sup> and detected by magnetoresistance effects<sup>13</sup>, and therefore can be implemented into nano-devices. Our findings provide a fundamental understanding of the oscillation nature of spin structures and its dependency on the shape and dimension of spin structures, which would be essential information for the development of nano-oscillator and also bio-inspired devices utilizing the oscillation.

## Materials and methods

### Sample fabrication

The electrode of Ti (5 nm)/Au (50 nm) was fabricated on a 100 nm thick X-ray transparent silicon-nitride (Si<sub>3</sub>N<sub>4</sub>) membrane to apply an oersted field. On the electrode, Py circular disk was deposited using the dc sputtering. The circular disk of a diameter  $D = 3 \mu\text{m}$ , and a thickness  $h = 100 \text{ nm}$  was patterned by electron-beam lithography and lift-off processing.

### X-ray imaging and time-resolved measurement

The magnetization components in a Py circular disk were directly observed by utilizing full-field magnetic transmission X-ray microscopy (MTXM) at XM-1 beamline 6.1.2 the Advanced Light Source (ALS). Out-of-plane magnetic components were imaged at the Fe L<sub>3</sub> X-ray absorption edge (708 eV). To image out-of-plane magnetic components, samples mounted with respect to the X-ray propagation direction. The MTXM contrasts represent a projection of out-of-plane magnetic components along the thickness direction. The images were normalized by an image with opposite photon helicity to enhance the MTXM contrasts.

The time-resolved measurement for X-ray imaging of dynamic behavior of vortex core structures was performed by utilizing the stroboscopic pump-probe technique at two-bunch mode of the ALS where X-ray is injected with the frequency of 3.33 MHz. We injected the Gaussian pulse of the amplitude  $V_{pp} = 2 \text{ V}$  and pulse width of 1.12 ns in Au electrodes. The injected pulse generates an oersted field pulse of the amplitude of 1 mT and a pulse width of 1.12 ns along  $-x$ -axis to excite the dynamic motion of vortex core structures in a Py circular disk. By tuning the delay time between pump (field pulse) and probe (X-ray pulse), the time-resolved MTXM images are measured.

### Micromagnetic simulation

To specify the detailed magnetization configurations of spin structures and its dynamics, we carried out the micromagnetic simulation by using mumax<sup>3</sup> code<sup>45</sup> that can solve numerically the Landau-Lifshitz-Gilbert (LLG) equation:  $\partial\mathbf{M}/\partial t = -\gamma_0(\mathbf{M} \times \mathbf{H}_{\text{eff}}) + (\alpha/|\mathbf{M}|)(\mathbf{M} \times \partial\mathbf{M}/\partial t)$  with the local magnetization vector  $\mathbf{M}$ , the gyromagnetic ratio  $\gamma_0$ , the effective field  $\mathbf{H}_{\text{eff}}$ , and the phenomenological damping constant  $\alpha$ <sup>55,56</sup>. We employed a Py circular disk of a diameter  $D = 3 \mu\text{m}$  and a thickness  $h = 100 \text{ nm}$  with the mesh size of  $4 \times 4 \times 4 \text{ nm}^3$ , which has exactly same dimension with the disk measured in our experiments. We used the typical material parameters of Py, i.e., saturation magnetization  $M_s = 800 \text{ kA/m}$ , exchange stiffness  $A_{\text{ex}} = 13 \text{ pJ/m}$ , and damping constant  $\alpha = 0.01$ . To excite the dynamic motion of vortex core structure, we applied Gaussian field pulses with the amplitude of 1 mT and the pulse width of 1.12 ns in  $-x$ -axis.

### Capturing position and area of vortex core structures in MTXM images

To analyze the dynamics of spin structures quantitatively, MTXM contrasts were processed by Gaussian fitting. After Gaussian fitting, we normalized the MTXM contrasts. For the 1D vortex core structures ( $H_x = 0$ , and 12 mT), the area of the vortex core structure was defined as the area where the normalized MTXM contrast is



smaller than 0.2. The position of the vortex core structure was determined as the centre of mass of the area of the vortex core structure. For the 2D vortex core structure ( $H_x = 24$  mT), we captured the position of the 2D vortex core structure, the minimum value of MTXM contrasts.

### Fast fourier transformation (FFT)

In experiments, we obtained FFT power spectra for the 1D and 2D vortex core structures with the frequency resolution of 0.091 GHz by performing fast Fourier transformation (FFT) of position of VC<sub>2</sub> and VC<sub>3</sub> structures during dynamic motion taken by MTXM measurements (Fig. 3c). To specify the oscillation mode of vortex core structures depending on the shape and dimension, by utilizing micromagnetic simulation, we applied the additional in-plane magnetic field with an amplitude of 1 mT to shift the vortex core structures from the initial position under static in-plane field  $H_x$  in the  $x$ -axis and turned off the additional magnetic field. We obtained FFT power spectra with the frequency resolution of 0.01 GHz by performing FFT of the oscillation of magnetization vector at each discrete cell with varying  $H_x$ .

### Acknowledgements

Works at the ALS were supported by the U.S. Department of Energy (DE-AC02-05CH11231). J.-I.H. was supported by the National Research Foundation of Korea (NRF) grant funded by Korea government (MSIT) (2020R1A2C2005932). K.-S.L. was supported by the NRF grant funded by Korea government (MSIT) (2019R1A2C2002996, and 2020M3F3A2A03082987), and was funded by the 2022 Research Funds (1.220024.01, and 1.220125.01) of UNIST (Ulsan National Institute of Science and Technology). M.-Y.I. acknowledges support by Lawrence Berkeley National Laboratory through the Laboratory Directed Research and Development (LDRD) Program.

### Author details

<sup>1</sup>Center for X-ray Optics, Lawrence Berkeley National Laboratory, Berkeley, CA 94720, USA. <sup>2</sup>Department of Materials Science and Engineering, Ulsan National Institute of Science and Technology (UNIST), Ulsan 44919, Republic of Korea. <sup>3</sup>Department of Emerging Materials Science, Daegu Gyeongbuk Institute of Science and Technology (DGIST), Daegu 42988, Republic of Korea. <sup>4</sup>Advanced Light Source, Lawrence Berkeley National Laboratory, Berkeley, CA 94720, USA. <sup>5</sup>Department of Physics, Chungbuk National University, Cheongju 28644, Republic of Korea

### Author contributions

H.-S.H., M.-Y.I., K.-S.L. designed and planned the research. H.-S.H., S.L., M.-S.J., N.K., M.K., H.-J.O., Y.-S.Y., M.-Y.I., K.-S.L. performed the experiments. H.-S.H., S.L., M.-S.J., Y.-S.Y., W.C., J.-I.H. prepared the samples. H.-S.H., M.-Y.I., K.-S.L. analyzed data. K.-S.L., H.-S.H. carried out the micromagnetic simulations. H.-S.H., M.-Y.I., K.-S.L. prepared the paper, which incorporates critical input from all authors.

### Data availability

The data that support the findings of this study are available from the corresponding author upon reasonable request.

### Conflict of interest

The authors declare no competing interests.

### Publisher's note

Springer Nature remains neutral with regard to jurisdictional claims in published maps and institutional affiliations.

**Supplementary information** The online version contains supplementary material available at <https://doi.org/10.1038/s41427-022-00438-9>.

Received: 10 March 2022 Revised: 3 September 2022 Accepted: 6 September 2022

Published online: 25 November 2022

### References

- Liu, G. et al. A charge-density-wave oscillator based on an integrated tantalum disulfide–boron nitride–graphene device operating at room temperature. *Nat. Nanotechnol.* **11**, 845–850 (2016).
- Zhu, C. et al. Light-Tunable 1T-TaS<sub>2</sub> Charge-Density-Wave Oscillators. *ACS Nano* **12**, 11203–11210 (2018).
- Zong, A. et al. Ultrafast manipulation of mirror domain walls in a charge density wave. *Sci. Adv.* **4**, eaau5501 (2019).
- Doiron-Leyraud, N. et al. Quantum oscillations and the Fermi surface in an underdoped high-T<sub>c</sub> superconductor. *Nature* **447**, 565–568 (2007).
- Goteti, U. S., Zaluzhnyy, I. A., Ramanathan, S., Dynes, R. C. & Frano, A. Low-temperature emergent neuromorphic networks with correlated oxide devices. *P. Natl. Acad. Sci. U S A* **118**, e2103934118 (2021).
- Kim, Y.-J., Jung, H., Han, S. W. & Kwon, O.-H. Ultrafast Electron Microscopy Visualizes Acoustic Vibrations of Plasmonic Nanorods at the Interfaces. *Matter* **1**, 481–495 (2019).
- Sie, E. J. et al. An ultrafast symmetry switch in a Weyl semimetal. *Nature* **565**, 61–66 (2019).
- Choe, S. B. et al. Vortex Core-Driven Magnetization Dynamics. *Science* **304**, 420 (2004).
- Yu, Y.-S. et al. Resonant amplification of vortex-core oscillations by coherent magnetic-field pulses. *Sci. Rep.* **3**, 1301 (2013).
- Satywali, B. et al. Microwave resonances of magnetic skyrmions in thin film multilayers. *Nat. Commun.* **12**, 1909 (2021).
- Dussaux, A. et al. Large microwave generation from current-driven magnetic vortex oscillators in magnetic tunnel junctions. *Nat. Commun.* **1**, 8 (2010).
- Yoo, M.-W. et al. Pattern generation and symbolic dynamics in a nanocontact vortex oscillator. *Nat. Commun.* **11**, 601 (2020).
- Pribiag, V. S. et al. Magnetic vortex oscillator driven by d.c. spin-polarized current. *Nat. Phys.* **3**, 498–503 (2007).
- Marković, D. & Grollier, J. Quantum neuromorphic computing. *Appl. Phys. Lett.* **117**, 150501 (2020).
- Liu, H. et al. A Tantalum Disulfide Charge-Density-Wave Stochastic Artificial Neuron for Emulating Neural Statistical Properties. *Nano Lett.* **21**, 3465–3472 (2021).
- Romera, M. et al. Vowel recognition with four coupled spin-torque nano-oscillators. *Nature* **563**, 230–234 (2018).
- Torrejon, J. et al. Neuromorphic computing with nanoscale spintronic oscillators. *Nature* **547**, 428–431 (2017).
- Grollier, J. et al. Neuromorphic spintronics. *Nat. Electron.* **3**, 360–370 (2020).
- Jung, H. et al. Logic Operations Based on Magnetic-Vortex-State Networks. *ACS Nano* **6**, 3712–3717 (2012).
- Ma, F., Zhou, Y., Braun, H. B. & Lew, W. S. Skyrmion-Based Dynamic Magnonic Crystal. *Nano Lett.* **15**, 4029–4036 (2015).
- Hubert, A. & Schäfer, R. *Magnetic Domains: The Analysis of Magnetic Microstructures*. (Springer, 1998).
- Guslienko, K. Y. et al. Eigenfrequencies of vortex state excitations in magnetic submicron-size disks. *J. Appl. Phys.* **91**, 8037–8039 (2002).
- Metlov, K. L. & Guslienko, K. Y. Stability of magnetic vortex in soft magnetic nano-sized circular cylinder. *J. Magn. Magn. Mater.* **242–245**, 1015–1017 (2002).
- Van Waeyenberge, B. et al. Magnetic vortex core reversal by excitation with short bursts of an alternating field. *Nature* **444**, 461–464 (2006).
- Kammerer, M. et al. Magnetic vortex core reversal by excitation of spin waves. *Nat. Commun.* **2**, 279 (2011).
- Cowburn, R. P. Change of direction. *Nat. Mater.* **6**, 255–256 (2007).
- Yamada, K. et al. Electrical switching of the vortex core in a magnetic disk. *Nat. Mater.* **6**, 270–273 (2007).
- Ivanov, B. A. & Zaspel, C. E. High Frequency Modes in Vortex-State Nanomagnets. *Phys. Rev. Lett.* **94**, 027205 (2005).
- Novosad, V. et al. Magnetic vortex resonance in patterned ferromagnetic dots. *Phys. Rev. B* **72**, 024455 (2005).

30. Finizio, S. et al. Control of the gyration dynamics of magnetic vortices by the magnetoelastic effect. *Phys. Rev. B* **96**, 054438 (2017).
31. Filianina, M. et al. Piezo-electrical control of gyration dynamics of magnetic vortices. *Appl. Phys. Lett.* **115**, 062404 (2019).
32. Lee, K.-S. & Kim, S.-K. Two circular-rotational eigenmodes and their giant resonance asymmetry in vortex gyrotropic motions in soft magnetic nanodots. *Phys. Rev. B* **78**, 014405 (2008).
33. Ding, J., Kakazei, G. N., Liu, X. M., Guslienko, K. Y. & Adeyeye, A. O. Intensity inversion of vortex gyrotropic modes in thick ferromagnetic nanodots. *Appl. Phys. Lett.* **104**, 192405 (2014).
34. Han, H.-S., Lee, S., Jung, D.-H., Kang, M. & Lee, K. S. Chirality-dependent asymmetric vortex core structures in a harmonic excitation mode. *Appl. Phys. Lett.* **117**, 042401 (2020).
35. Lv, G., Zhang, H., Cao, X., Gao, F. & Liu, Y. Micromagnetic simulations of magnetic normal modes in elliptical nanomagnets with a vortex state. *Appl. Phys. Lett.* **103**, 252404 (2013).
36. Noske, M. et al. Three-dimensional Character of the Magnetization Dynamics in Magnetic Vortex Structures: Hybridization of Flexure Gyromodes with Spin Waves. *Phys. Rev. Lett.* **117**, 037208 (2016).
37. Guslienko, K. Y., Kakazei, G. N., Ding, J., Liu, X. M. & Adeyeye, A. O. Giant moving vortex mass in thick magnetic nanodots. *Sci. Rep.* **5**, 13881 (2015).
38. Yoo, M.-W., Lee, J.-H. & Kim, S.-K. Excited eigenmodes in magnetic vortex states of soft magnetic half-spheres and spherical caps. *J. Appl. Phys.* **116**, 223902 (2014).
39. Boust, F. & Vukadinovic, N. Micromagnetic simulations of vortex-state excitations in soft magnetic nanostructures. *Phys. Rev. B* **70**, 172408 (2004).
40. Yan, M., Hertel, R. & Schneider, C. M. Calculations of three-dimensional magnetic normal modes in mesoscopic permalloy prisms with vortex structure. *Phys. Rev. B* **76**, 094407 (2007).
41. Ding, J., Kakazei, G. N., Liu, X., Guslienko, K. Y. & Adeyeye, A. O. Higher order vortex gyrotropic modes in circular ferromagnetic nanodots. *Sci. Rep.* **4**, 4796 (2014).
42. Buchanan, K. S. et al. Magnetic-field tunability of the vortex translational mode in micron-sized permalloy ellipses: Experiment and micromagnetic modeling. *Phys. Rev. B* **74**, 064404 (2006).
43. Yakata, S., Tanaka, T., Kiseki, K., Matsuyama, K. & Kimura, T. Wide range tuning of resonant frequency for a vortex core in a regular triangle magnet. *Sci. Rep.* **3**, 3567 (2013).
44. Fischer, P. et al. Soft X-ray microscopy of nanomagnetism. *Mater. Today* **9**, 26–33 (2006).
45. Vansteenkiste, A. et al. The design and verification of MuMax3. *AIP Adv.* **4**, 107133 (2014).
46. Han, H.-S. et al. Topology-dependent stability of vortex-antivortex structures. *Appl. Phys. Lett.* **118**, 212407 (2021).
47. Mayr, S. et al. Spin-Wave Emission from Vortex Cores under Static Magnetic Bias Fields. *Nano Lett.* **21**, 1584–1590 (2021).
48. Im, M.-Y. et al. Dynamics of the Bloch point in an asymmetric permalloy disk. *Nat. Commun.* **10**, 593 (2019).
49. Graf, J., Pfeifer, H., Marquardt, F. & Viola Kusminskiy, S. Cavity optomagnonics with magnetic textures: Coupling a magnetic vortex to light. *Phys. Rev. B* **98**, 241406 (2018).
50. Cheynis, F. et al. Controlled Switching of Néel Caps in Flux-Closure Magnetic Dots. *Phys. Rev. Lett.* **102**, 107201 (2009).
51. Masseboeuf, A. et al. Dimensionality Crossover in Magnetism: From Domain Walls (2D) to Vortices (1D). *Phys. Rev. Lett.* **104**, 127204 (2010).
52. Yu, X. W. et al. Images of a Spin-Torque-Driven Magnetic Nano-Oscillator. *Phys. Rev. Lett.* **106**, 167202 (2011).
53. Lee, K.-S. & Kim, S.-K. Conceptual design of spin wave logic gates based on a Mach-Zehnder-type spin wave interferometer for universal logic functions. *J. Appl. Phys.* **104**, 053909 (2008).
54. Behncke, C. et al. Spin-wave interference in magnetic vortex stacks. *Commun. Phys.* **1**, 50 (2018).
55. Gilbert, T. L. A Lagrangian formulation of the gyromagnetic equation of the magnetization field. *Phys. Rev.* **100**, 1243 (1955).
56. Landau, L. D. & Lifshitz, E. M. On the theory of the dispersion of magnetic permeability in ferromagnetic bodies. *Phys. Z. Sowjetunion* **8**, 153–164 (1955).